A physics-based rock-friction constitutive law, part II: predicting the Brittle-Ductile Transition.

Einat Aharonov[1] and Christopher H. Scholz[2]

[1] Institute of Earth Sciences, The Hebrew University, Jerusalem, 91904, Israel

[2] Lamont-Doherty Earth Observatory of Columbia University, Palisades, New York, USA

Corresponding author: Einat Aharonov (einatah@mail.huji.ac.il)

Key Points:

- The friction model from "A physics-based rock-friction constitutive law, part I" is extended to high ambient temperature & pressure
- We allow real contact area to saturate when it reaches high enough values. Saturation instigates a friction-plastic transition.
- Experimentally observed friction/strength at high T & pressure are predicted. We discuss implications to the brittle-ductile transition.

Abstract

The 1st paper of this series introduced a model of rock friction based on asperity contacts deforming by low temperature plasticity creep laws for both the shear and contact-normal modes. There we showed that the properties of rock friction at low ambient temperature and pressure over a very wide range of sliding velocities could be predicted using independently determined parameters. The real contact area, A_r, increases with normal stress, temperature, and time. Here we argue that at high ambient temperatures and pressures there is a maximum real contact area A_r^{max}. This defines a point beyond which the shear strength becomes independent of the normal stress and the rheology changes from frictional to plastic, viz. the frictional-plastic transformation. Using the same parameters as in paper 1, we determine the sole free parameter A_r^{max} by fitting the model to experimental data on friction of granite at high temperature, pressure, and various sliding rates. We then apply the model to the natural tectonic conditions in the Earth, in which it predicts that the frictional-plastic transition occurs in a wet quartzo-felspathic crust at approximately 300° C, weakly dependent on fault slip rate. Below this depth stress decreases linearly with depth following an exponential plastic flow law until approximately 500°C, where the transition to high temperature power law creep occurs. Thus the brittle-ductile transition is gradual and occurs over a span of about 200°C, from about 300 to 500° C, in agreement with experimental and field observations of the brittle-ductile transition for quartz.

1 Introduction

i. The nature of the brittle-ductile transition.

Geological observations indicate that the upper crust deforms by frictional faulting whereas the lower crust deforms by crystal plastic flow. Thus a simplified strength envelop for the crust was devised by combining a linear Coulomb friction law to describe the limiting stress of faulting with a power law creep law for the plastically deforming lower crust *[Brace and Kohlstedt, 1980; Goetze and Evans, 1979]*. The point where these two curves meet is said to define the brittle-ductile transition (BDT). The BDT is also assumed to define the lower limit of seismic activity on active faults. The prediction of the BDT of this two-mechanism model corresponds reasonably well with the depth distribution of earthquakes on continental faults *[Sibson, 1982]* as well as the depth of the transition from cataclasite to mylonite associated with the onset of quartz plasticity in fault zones cutting quartzo-feldspathic rock *[Stipp et al. 2002; Voll 1976; White et al 1980]*. A smoothed version was developed by *Shimamoto and Noda (2014)* and was used to explain halite data.

However, it is clear that this description is overly simplistic. For one thing, the power law creep law that is extrapolated from high temperature lab measurements is not expected to be the flow regime at the low temperatures and high stresses near the BDT. In addition, both experimental *[Hirth and Tullis, 1992]* and field observations *[Stipp et al., 2002]* show that the BDT does not occur at a point but is a gradual transition involving an evolution of deformation mechanisms over a depth range corresponding to several hundred °C. The experimental and field studies of quartz deformation find three regimes with increasing temperature: an onset of plasticity associated with dislocation glide and negligible climb and recovery, an intermediate mixed mode of deformation, and a high temperature regime characterized by rapid dislocation climb and recovery. At geological strain rates, the first regime begins at ~ 300°C and the third regime at ~ 500°C *[Stipp et al., 2002]*. Although it is hazardous to identify micro-mechanisms with rheology, it is fair to say that power law creep, which fundamentally depends upon dislocation climb, can only be associated with the highest temperature of these three regimes. The lowest temperature regime, at the onset of plasticity, must be associated with a flow law that allows thermally activated glide without rapid enough atomic diffusion to permit climb and recovery. A rheology of this type, often called Peierls creep, which typically describes low temperature, high stress plasticity, is of the form *[e.g. Chester 1994, Evans and Goetze 1979, Tsenn and Carter 1987]*

$$\dot{\varepsilon} = A\exp(-[Q - \tau\Omega]/RT) \qquad (1)$$

Mei et al (2010), in a strength model for the oceanic lithosphere, included a layer with a rheology of this type between the frictional and power law creep regimes.

These two or three-mechanism models are not theories of the BDT, merely criteria that constrain its position. A theory of the BDT must include a mechanism that explicitly predicts it. Here we provide such a theory, based on a model of friction in which the deformation at the contact scale follows a flow law of the form of eqn. 1, as detailed in the companion paper in this issue, paper 1. It is fundamental to such a model that the real area of contact, A_r, increases with normal stress and temperature and with decreasing slip rate. Yet it is clear that the normalized real contact area (A_r/A) cannot increase beyond 1. At some point A_r must reach a maximum value A_r^{max} in which the ratio $A_r^{max}/A \leq 1$. We claim, and show below, that once $A_r = A_r^{max}$ the shear strength will no longer increase with normal stress but will remain constant, and the rheology will change from friction to a plastic flow law of the form (1). This point predicts the onset of the BDT zone– the frictional-plastic transition. The lower limit of the BDT zone occurs where the exponential flow law intersects the power law creep law.

ii. The goal of this work

In Paper 1 we derived a single, physics-based, friction law to explain and predict steady-state friction in rocks. This model is general for all shear velocities (V), temperatures (T), normal stresses (σ_n), and materials. Paper 1 tests this model for quartz and granite across a wide range of slip velocities, under low normal stress and low ambient temperatures. We found that our model explains and predicts the major features of rock friction over a range of slip rates from interseismic to coseismic velocities.

In this paper we use the same model and the same material parameters that were used in paper1 for the low T and low normal stress experiments, but under high ambient temperatures and high normal stress. We compare the model predictions with the high T and σ_n data for granite and quartzite of *Blanpied et al (1995)*, and *Chester and Higgs (1992)* (Fig 1). The only free parameter that remains to fitting these data is A_r^{max}. This parameter will be shown below to define both the frictional-plastic transition, and the dependence of friction on ambient temperature in the plastic regime. Applying these results to the continental crust show that the Brittle-Ductile Transition zone is a region several km thick with a lower bound given by the frictional-plastic transition and an upper bound at the transition from exponential creep to power law creep. Using the parameters determined by fitting the experimental data predicts a frictional-plastic transition at about 300°C, weakly dependent upon fault slip rate.

We argue that we may use quartz flow laws for granite, since at higher temperature the granite forms a mylonitic fabric where the quartz, which is plastically deforming, forms layers parallel to shear, separated by feldspar (which behaves rigidly) layers, so the deformation is controlled by the weaker quartz layers.

2) Theory

The first two assumptions of theory are detailed in sec 2 of paper1, and presented here again for brevity. The third assumption is a new one that is added here.

i. Assumption 1: Friction arises from creep of contacts, and is predictable from contact stresses

The model derived in paper1 assumes that macroscopic friction arises from simultaneous shear and normal creep on a population of sliding contacts, following *Bowden and Tabor (1956, 1964),* (abbr. B&T). It follows *Heslot et al.(1994), Brechet & Estrin (1994), Baumberger & Caroli (2006) , Rice et al (2001), Nakatani (2001) and Putelat et al (2011),* in assuming that contact shear strength, τ_c, for sliding at a given slip rate V is controlled by a flow law of the form of eqn. 1, on the contact-scale. Eqn (2a) of paper 1 writes this assumption for contacts sliding at velocity *V:*

$$(2)\ V = V_{smax}\exp(-\frac{Q_s-\tau_c N\Omega_s}{RT_c});$$

here N is Avogadro number, T_c is the contact temperature, R the gas constant, Q_s and Ω_s are the activation energy and activation volume for shear creep . V_{smax} is a reference velocity, the highest possible shear creep rate achieved when shear contact stresses, τ_c, is at its highest possible value $\tau_c=\tau_c^*=Q_s/N\Omega_s$, (see paper 1 for detailed explanation). Eqn 2 is easily inverted to give the contact shear stress, τ_c, as function of V, T_c and material parameters, providing eqn 3b below. Eqn 2c-2d of paper1 derived the contact normal stress, σ_c, using a similar creep law but in the normal direction to the contact, i.e. exponential normal creep causing contact convergence and contact area growth. From these assumptions, we obtained the shear (eqn 3b) and normal (eqn 3a) stresses on contacts in paper 1, there detailed in eqn 3a-e, and presented here again for completeness:

$$(3a)\qquad \sigma_c(t) = \sigma_c^0\left(1 - b'\ln\left(1+\frac{d}{Vt_c}\right)\right)$$

$$(3b)\qquad \tau_c(t) = \tau_c^*(1 + a'\,ln\left(\frac{V}{V_{smax}}\right))$$

$$(3c)\qquad \frac{A_r}{A} = \frac{\sigma_N}{\sigma_c^0}\frac{1}{\left(1 - b'\ln\left(1 + \frac{d}{Vt_c}\right)\right)}$$

$$(3d)\qquad a' = \frac{RT_c}{Q_s};\quad b' = \frac{RT_c}{BQ_v};\quad \sigma_c^0 = \frac{Q_v B}{N\Omega_v};\quad \tau_c^* = \frac{Q_s}{N\Omega_s};\quad E_{tc} = Q_v - N\Omega_v\sigma_c^0 = (1\text{-B})Q_v$$

$$(3e)\qquad t_c = b'\frac{d}{V_{nmax}}\exp\left(\frac{E_{tc}}{RT_c}\right)$$

The real contact area A_r, normalized by nominal area A, in eqn 3c, was derived from the relation $A_r\sigma_c = A\sigma_n$. The constants given in (3d) -(3e) were derived and their significance explained in paper 1. Their range of values are given in Table 1 of paper 1. For completeness they are briefly presented here: t_c is the "cutoff time" *(Nakatani and Scholz, 2004a,b),* which is thermally activated and has activation energy, E_{tc}. σ_c^0 is the contact stress at time *t=0,* meaning the stress at the birth moment of each contact. In Paper 1 it is called the 'indentation hardness' at time t=0. B is a prefactor between 0 and 1, whose value changes with temperature to account for the decrease of σ_c^0 with temperature, following experimental observations (*Evans 1984*, see discussion of this topic in Paper 1). V_{nmax} is reference, (highest possible), normal creep rate. Activation energy, Q_s, and activation volume, Ω_s, for surface creep, may differ from bulk volumetric creep parameters, Q_v and Ω_v. d is contact diameter. This is also discussed at length in paper 1.

From eqn 3, one may obtain the friction coefficient, $\mu = \frac{\tau_c}{\sigma_c}$, by dividing eqn 3b by eqn 3a. Since $A_r\sigma_c = A\sigma_n$, one may alternatively express the friction coefficient via the contact area instead of via σ_c.

$$4)\ \mu = \frac{A_r}{A}\frac{\tau_c}{\sigma_n}$$

This form better serves our purposes here, and eqn 4 will be used in this paper to obtain friction. Note that it is the full solution for friction, that holds for all temperatures, normal stresses and velocities.

ii. **Assumption 2: Steady-state temperature and friction.**

We assume sliding is steady when both friction and contact temperature reach steady-state. The steady-state temperature of the contacts (paper 1, eqn 5) is rewritten here for completeness:

$$5)\quad T_c = T_0 + \frac{\tau_c}{\rho C}\sqrt{\frac{V}{\pi\alpha}}\left[\sqrt{d} + \frac{\sigma_n}{\sigma_c}\sqrt{D_{th}}\right]$$

where T_0 is the ambient temperature, D_{th} the thermal distance over which the sliding surface achieves steady state *(DiToro et al 2011), C* is the heat capacity, α the thermal diffusivity, and ρ the density, see eqns 5-6 in paper1 for derivation, details and discussion.

When slip rate is fast enough (seismic), eqn (5) predicts that the contacts reach melting temperature, T_m. Thermodynamic considerations dictate that T can't exceed T_m, even if V is increased further. In this case we assume that steady-state sliding occurs at $T_c=T_m$, and that shear stress is reduced to compensate, following eqn (6) in paper 1.

iii. Assumption 3: plasticity onset when contact area saturates

When the ambient temperature and the applied normal stress are high, contact behavior changes and so does friction. In nature it is observed that above a certain ambient temperature and normal stress, the fault zone becomes a mylonite zone, i.e. the fault transits to fully plastic flow. To capture plastic flow physics in our model, we add now a single physical assumption, that at some point, at high enough σ_n, T_c, and t, the real area of contact, A_r, in eqn 3c, must reach a maximum value, A_r^{max}, such that it cannot increase further. Here we assume that A_r^{max} is a constant (which will be shown to fit the present data), but we cannot rule out the possibility that A_r^{max} depends on normal stress and ambient temperature.

We next predict theoretically that this assumption alone leads in our model to two fundamental findings: i) the point of contact area saturation coincides with the FPT (frictional-plastic transition) since it leads to constant shear strength that does not increase with normal stress, and ii) the rheology changes from frictional sliding, to a plastic flow law of the form of eqn (1). To demonstrate this, we calculate the friction of rocks at the two sides of the FPT from eqn 4. Eqn 4 gives the general form for friction, both during frictional and plastic deformation, since its derivation didn't decide yet what is A_r. The following shows that both frictional and plastic behaviors arise from eqn4 - frictional behavior occurs when A_r evolves, and plastic when A_r saturates to A_r^{max}

Frictional regime: In this regime A_r evolves with V and T_c according to eqn 3c. Plugging eqn 3c into the friction eqn 4 gives the steady-state friction coefficient in the frictional sliding regime, μ_{ss}^{f}:

$$(6a)\ \mu_{ss}^{f} = \frac{\tau_c^{*}\left(1 + a' ln\left(\frac{V}{V_{smax}}\right)\right)}{\sigma_c^{0}\left(1 - b' \ln\left(1 + \frac{d}{Vt_c}\right)\right)}$$

$$(6b)\ \mu_{ss}^{f} \sim \mu_0 + a \ln\left(\frac{V}{V_{smax}}\right) + b \ln\left(1 + \frac{d}{t_c V}\right)$$

$$(6c)\ \ a = a'\,\mu_0 = \mu_0 \frac{RT_c}{Q_s};\ \ b = b'\mu_0 = \mu_0 \frac{RT_c}{BQ_v};\ \ \mu_0 = \frac{\tau_c^{*}}{\sigma_c^{0}} = \frac{Q_s}{BQ_V}\frac{\Omega_V}{\Omega_S}$$

Which is identical to eqn (4) of paper 1. (We call the friction coefficient here μ_{ss}^{f}, although in paper 1 it is called simply μ_{ss}, to distinguish it here from the "plastic friction" μ_{ss}^{p} that will be discussed in the next subsection).

Eqn (6b) is identical to eqn (4b) of paper 1. The coefficient *a*, defined as the *viscous term* in paper1, comes from the shear stress dependence on V (eqn 3b). The coefficient b, termed the *contact area growth term* in paper 1, comes from the A_r dependence on V.

The shear strength in the frictional regime, τ_{ss}^{f}, is simply the friction coefficient in eqn (6b), μ_{ss}^{f} , multiplied by the applied normal stress σ_n:

$$6d)\ \tau_{ss}^{f} \sim \sigma_n \left(\mu_0 + a \ln\left(\frac{V}{V_{smax}}\right) + b \ln\left(1 + \frac{d}{t_c V}\right)\right)$$

Thus the shear strength in the frictional regime increases linearly with applied normal stress.

Plastic regime: here instead of the growth eqn for A_r (eqn (3c)), used in the frictional regime, we use $A_r = A_r^{max}$ in eqn 4. Again the expression eqn 3b is used for τ_c. In this regime the friction coefficient μ_{ss}^{p} and the shear strength τ_{ss}^{p} are :

$$(7a)\ \ \mu_{ss}^{p} = \mu_0^{p} + a\ ln\left(\frac{V}{V_{smax}}\right)$$

$$(7b)\ \ \mu_0^p = \frac{A_r^{max}}{A\sigma_n}\frac{Q_s}{N\Omega_s}; \qquad a = \frac{A_r^{max}}{A\sigma_n}\frac{RT_c}{N\Omega_s}$$

$$(7c)\ \ \tau_{ss}^p = \sigma_n\left(\mu_0^p + a\ ln\left(\frac{V}{V_{smax}}\right)\right) = \frac{A_r^{max}}{AN\Omega_s}\left(Q_s + RT_c\ ln\left(\frac{V}{V_{smax}}\right)\right)$$

Eqn 7 shows that in the plastic regime steady-state friction and strength are only controlled by the viscous term (the *a* term), while the *b* term (the *contact area growth term*) dropped out. Friction (eqn 7a) and strength (eqn 7c) are always V-strengthening, and there is no velocity weakening in plastic flow, except that produced by increasing T_c during shear heating at high slip rate (as explained in the Discussion of paper 1).

Eqn 7c shows that the shear strength, τ^p, is in this case is independent of normal stress, which indeed is a property characteristic of plastic deformation.

Finally, we demonstrate that a plastic flow law of the form eqn(1) describes the plastic flow regime, by inverting eqn (7c) to obtain V as function of τ_{ss}^p:

$$(8) \qquad V = V_{smax}\exp\left(-\frac{Q_s - \frac{A}{A_r^{max}}N\Omega_s\,\tau_{ss}^p}{RT_c}\right)$$

Thus our model is expected to capture the plastic-behavior of rocks below the FPT.

3) Method and Parameter values

This paper explores our model for steady sliding under elevated ambient temperature, T_0, ranging between 0 - 600°C and applied normal stress, σ_n, ranging between 5 - 500 MPa, to probe conditions relevant for different depths in the Earths crust. Similar to paper 1, we numerically solve coupled eqns 3, 4 & 5 (and eqn 6 from paper 1 in case melting is reached), seeking a coupled dynamic steady-state solution for contact stresses and contact temperature, by iterative solutions using a Matlab subroutine that we wrote. Details of solution technique and treatment of melting contacts are given in paper 1.

The difference from paper 1 is that here we add the assumption of a saturation value for A_r, A_r^{max}. This assumption is added since, as opposed to paper 1 which tested only low stresses and ambient temperatures, this paper tests friction under high normal stresses and high ambient temperatures. These conditions are expected to considerably increase the value of real contact area relative to values in paper 1.

We use thermodynamically and mechanically constrained values of parameters, as detailed in paper1, for quartz and granite. Simulations were ran using the parameters of run4 from paper 1, as detailed in Table 1 below. Although at low T_0 the behavior of all the runs in paper 1 differed only slightly (see Figs 6 & 8 in paper1) the differences between runs are accentuated at higher T_0, and run 4 provided the best fit to the high T and stress experiments, as detailed below

Table 1 – table of parameters, definitions and values.

parameter	symbol	Value (run 4)	units	ref
volumetric activation volume	Ω_v	5	m^3	*Nakatani 2001, Rice 2001*
surface activation volume	Ω_s	7.8	m^3	“
Volumetric activation energy	Q_v	240	KJ/mol	“
Surface activation energy	Q_s	270	KJ/mol	“
Prefactor	B	0.89	-	here
Contact diameter	d	10	m	*Beeler et al 2008*
Maximum shear rate	V_{smax}	$0.5c_s$		*Noda 2008, Rice 2001*
Shear wave velocity	c_s	3750	m/s	www.quartz.com
Reference cutoff time, at room T	t_{cr}	2	s	*Dieterich 1972,1978,*
Thermal equilibration distance.	D_{th}	$C\sigma_n^q$, here C=5, q = -1.	m	*DiToro et al 2011, 2004*
Melting temperature	T_m	1670	K	*Rice 2006*
Ambient temperature	T_0	270-870	K	imposed
Heat capacity	C	730*(1.7-200/Tc)	J/kg/K	Fitting fig 4 of *Vosteen & Schellschmidt 2003*

Thermal diffusivity	α	10^{-4}/T – $0.5*10^{-7}$	m^2/s	fitting Fig4 of *Hanley et al, 1978,* assuming 1-OM reduction by porosity
Density	ρ	2650	Kg/m^3	
Contact temperature	T_c	300-2000	K	from eq 5
Shear rate	V	10^{-13}-10	m/s	Imposed.
Saturated contact area	A_r^{max}	0.095	-	here
Applied normal stress	σ_n	5-500	MPa	
Steady-state friction coef	μ_{ss}	0.01-1	-	from eqn 4
Shear stress on contacts	τ_c	(0.01-0.18) G	MPa	from eqn 3
Normal stress on contacts	σ_c	(0.1-0.22) G	MPa	from eqn 3
viscous prefactor	a	0.0075-0.0225	-	from eqn 3
Contact-growth prefactor	b	0.012-0.0282	-	from eqn 3
Avogadro number	N	$6 * 10^{23}$	1/mol	
Gas constant	R	8.3	J/mol/K	
Shear modulus	G	$31\ 10^9$	Pa	

4) Results

i. Steady-state friction at elevated temperatures and normal stresses

We first model steady sliding friction at three different slip rates, as function of T_0 (between 0 - 550°C), under σ_n=400MPa, to compare with the *Blanpied et al (1995)* experimental data of granite friction presented in Fig1a. In fitting the data, we use the parameters of run4 (paper 1 and Table 1). The only free parameter in our model is A_r^{max}, determined by data fitting. Fig 2a presents the experimental data (symbols) together with our model results using $A_r^{max}/A = 9.5\%$. Note that in this figure the ordinate is labeled friction, but it really represents shear stress divided by a constant value of normal stress of 400 MPa. Below the FPT it can properly be interpreted as the friction coefficient; above it describes the plastic shear strength, the value of which is that number times 400 MPa

Figure 2a shows that the model fits the entire dataset. It predicts that friction increases with T_0 up to a peak value that corresponds to the FPT. Within that region friction has only a minor dependence on velocity, as expected from R/S friction. Above that point, which we define as T_{FPT}, the theory accurately predicts the strong weakening with temperature and the strong velocity strengthening observed in the data. Figure 2b shows the inner workings of the model with a plot of A_r/A vs. T_0. A_r/A increases with T_0 until A_r^{max} is reached, then remains constant. The value of T_0 where A_r reaches its maximum is $T_{FPT.}$ T_{FPT} increases with velocity because at higher velocity there is less time for A_r to grow at a given T_0.

Changing the sole free parameter, $\frac{A_r^{max}}{A}$, has two effects on the model curves: first it shifts T_{FPT} left or right, and second it changes the slope of friction (or strength) vs ambient temperatures both below and above the FPT. Above the FPT the effect of $\frac{A_r^{max}}{A}$ on the slope, $\frac{\partial \tau_{ss}^p}{\partial T_c}$, for $T>T_{FPT}$ may be predicted by taking a derivative of eqn (7c):

$$(9) \quad \frac{\partial \tau_{ss}^p}{\partial T_c} = \frac{A_r^{max}}{A} \frac{R}{N\Omega_s} ln\left(\frac{V}{V_{smax}}\right).$$

Eqn (9) predicts that at a given slip rate, the slope of the strength with respect to T_0 is linear (assuming $A_r^{max} = const$), negative (since $V<V_{smax}$), and changes with slip rate: curves becomes increasingly negative with decreasing V, in agreement with the data in fig 2. The linear slope depends on several very tightly constrained parameters (σ_n, N, R) and on several less tightly constrained parameters ($\frac{A_r^{max}}{A}, \Omega_s, V_{smax}$). The values of activation volume, Ω_s, and V_{smax} were discussed in paper1, and constrained in the different runs presented there for the low T_0 and σ_n experiments. This leaves here only A_r^{max}/A as the sole free parameter to constrain the linear slopes of strength vs T_0 within the curves in Fig 2. Trying to fit all the runs from paper 1 suggests run 4 best fits the data, with all the rest of the runs showing poorer fits. Given the uncertainty in Ω_s, and V_{smax} the slope of the curves in Fig 2 constrains $\frac{A_r^{max}}{A} = 0.1 \pm 0.02$. In addition to fixing

the slopes, once set, the same $\frac{A_r^{max}}{A}$ controls also the position of $T_{FPT.}$ The excellent agreement between the *Blanpied et al (1995)* experiments and our simulations lends confidence to our model and the derived value of $\frac{A_r^{max}}{A}$, given the fact that the model fits 3 non-monotonic curves with only one (semi-) free parameter (semi-free since $0 < \frac{A_r^{max}}{A} < 1$), and since once it is chosen to fit a single slope at $T>T_{FPT}$, $\frac{A_r^{max}}{A}$ cannot be tuned further to adjust the locations of T_{FPT}, and to fit the other curves for the other slip rates.

We also modeled friction under the *Blanpied et al (1995)* experimental conditions for slip at other rates, in addition to the three slip rates shown in Fig 2. Fig 3a plots friction as function of slip rate at 400Mpa, with different curves representing sliding at different ambient temperatures, ranging from room temperature to 530C. Model results show that at $T_0 < 230^oC$ sliding is still fully frictional, following the frictional behavior explored in paper1. Plasticity starts to appear at $T_0=230^oC$, but only at very slow slip rates -- $V< 10^{-9}$ m/s. A plastic to friction transition occurs at $V=10^{-9}$ m/s, and is observed here via a change in slope of friction as function of velocity: While the frictional slip at $V> 10^{-9}$ m/s is V-weakening, for $V<10^{-9}$ m/s plastic slip produces strong velocity strengthening (as predicted in eqn 7). We term the velocity at which the plastic to frictional transition occurs at a given $T_{0,}$ $V_{FPT}(T_0)$. V_{FPT} increases rapidly with ambient temperature: $V_{FPT}(230C)$~10^{-9} m/s, $V_{FPT}(330C)$~10^{-7} m/s, while $V_{FPT}(430C)$~10^{-5} m/s. At $T_0=530^oC$ sliding is fully plastic at all slip rates we tried. Even though sliding is fully-plastic at all V for this T_0, we see that not all slip rates are V-strengthening. The V-weakening observed at high V in the plastic regime arises from thermal softening due to shear heating effects, as explained in sec 6.f of paper1. Our predictions agree with the experimental results of *Chester and Higgs (1992*), (presented here in Fig 1b), showing similar abrupt inversion of slope at the FPT, and similar increase in V_{FPT} with increasing $T_{0.}$

Fig 3b shows the relative contact area, A_r/A, as function of slip rate for the runs in Fig 3a. The red dashed line depicts the value of saturated contact area, $A_r^{max}/_A$, obtained by fitting our model to the experimental curves in Fig 2. Fig 3b shows that at low ambient temperatures, T_0<230C, contact area varies with slip rate, since slip is fully frictional. For T_0>230C, at low enough slip rates, the elevated T_0 and the long contact duration during slow sliding, allow A_r to reach its saturation value A_r^{max}. This is the reason for the plastic regime at the very low slip rates. Increasing T_0 even further enhances contact growth (eqn 3), so plastic slip dominates sliding at increasingly larger slip rates, until at T_0=530^{o}C sliding occurs always at saturated contact area, independent of slip rate.

We next explore the FPT and behaviors on both sides of it by obtaining the shear strength, τ, as function of applied normal stress σ_n for various slip rates and various ambient temperatures T_0. Here τ was calculated from multiplying the friction coefficient in eqn 4 by σ_n. Model results are presented in Fig 4. The FPT appears as a transition from a linear relation between τ and σ_n (i.e. frictional behavior) prevailing at low σ_n, (eqn 6d) to sliding at constant τ, independent of σ_n, at high σ_n (eqn 7c). The normal stress at which FPT occurs increases with decreasing T_0, and with increasing slip rate V. For example, at T_0 =200^{o}C plasticity appears at ~400MPa when sliding at V= 0.001 μm/s, but no plasticity is seen (up to 500MPa &500 ^{o}C) when sliding faster. At $T_{0=}$400^{o}C plasticity appears at ~300Mpa for V= 0.001 μm/s, and at ~400Mpa for V= 1μm/s. The physics for the normal stress dependence of the FPT is the same as that controlling the temperature dependence of the FPT seen in the experiments of *Chester and Higgs (1992)*, (here in Fig 1b) and in Fig 2.

ii. Steady-state friction as function of depth in the crust

We used our model to simulate friction at normal stress and temperature values representing different depths in the crust. T_0 and σ_n were calculated using geothermal gradient of 25^{o}C/km and effective normal stress gradient of 18MPa/km, implying 27 MPa/Km for lithostatic stress minus hydrostatic pore pressure. This is appropriate for thrust or strike-slip faulting coincident with thrusting. Fig 5 plots friction as function of slip rate, where the different curves are calculations at depths of 6, 10, 11, 13 and 15 Kms. The dependence of friction on slip rate varies with depth. Descending from the surface to 10kms the absolute value of the friction coefficient increases, but it also becomes increasingly V-weakening with depth (i.e friction is more V-weakening at 10kms than at 6km). Plasticity starts at 11kms, but it has a unique form: while at very low slip rates, for V< 10^{-10} m/s, slip is plastic and V-strengthening, slip remains frictional at higher slip rates. This is the same behavior as seen and explained in Fig 3.

Descending deeper into the curst, plasticity prevails to higher and higher slip rates, until at ~15kms, slip becomes fully plastic at all rates. However, even for this fully plastic slip, strength does not monotonically increase with V as expected from plastic flow at constant temperature: at high enough sliding rate, when V exceeds the thermal velocity V_t (here ~5 μm/s), friction undergoes thermal softening. The thermal velocity V_t is defined and discussed in paper 1.

5. The Brittle-Ductile transition zone in the earth

i. The Brittle-Ductile Transition Calculated from Theory

We may use our model to gain new insight regarding the Brittle-Ductile transition in the Earths crust. Fig 6 plots shear strength for faults with 3 different geological slip rates as function of depth. It plots our calculations from our friction law which exhibits the friction-plastic transition and the exponential flow law beyond it (solid lines). We then extrapolate the experimental flow law for power law creep of wet quartzite *(Hirth et al, 2001*) to determine the lower boundary of the Brittle Ductile Transition.

T_0 and σ_n were calculated using geothermal gradient of 25°C/km and normal stress gradient of 18MPa/km. The 3 slip rates we used, noted in mm/yr, are 0.3, 3 and 30 mm/yr, represent geologic slip rates for active faults. These rates correspond to slow intraplate, fast intraplate, and interplate faults, respectively. These velocities are converted to strain rates in the plastic shear zones, assuming their thickness is in the range of several hundred meters to a km *(e.g., Stipp et al 2002, Beeler et al, 2016).* (The width of the shear zones are assumed to increase with slip rate because that usually correlates with total slip and the width of shear zones generally increases with net slip (e.g. *Hull, 1988*).

Our model predicts two regimes: strength of the shallow crust follows a nearly linear friction law, as in Byerlee, eqn 6d. The linear dependence of τ with depth is dictated by the linearly increasing $\sigma_n.\mu_0$ dominates and the a and b terms are small in comparison, so their increase with temperature contributes only a very slight concavity to the lower part of the curves.

Strength peaks at around 10-14 kms (depending on slip rate and on the geotherm assumed) where transition to plasticity occurs due to saturated contact area. This ductility is low temperature plasticity, occurring via exponential creep of contacts. It has a different dependence on depth than power-law flow. The exponential creep follows a linear strength drop with depth. The RHS of Eqn 7d, the plastic strength law, explains why: strength is independent of normal stress (see also fig 4). The dependence of strength on depth in this plastic regime is only due to the *a* pre-factor, that grows linearly with temperature. Since ln(V/V_{smax})<0, the *a* term becomes increasingly negative as T grows, reducing strength linearly with depth following our linear geotherm. Exponential creep then extends down until it intersects the power-law creep flow law, depicted as dashed lines, calculated from the quartzite power law creep law derived from experiments *(Hirth et al, 2001).* The dashed lines are inversion of the power law to obtain stress from strain rate.

$$(10) \quad \tau = \left(\frac{\dot{\varepsilon}}{k f_{H_2O}^{m}}\right)^{\frac{1}{n}} \exp\left(\frac{Q}{nRT}\right)$$

here $\dot{\varepsilon}$ is strain rate, taken as 10^{-14}, 10^{-13}, 10^{-12} 1/s, from assuming 0.3, 3, and 30 mm/yr slip distributed over a shear zone that is 100m, 300m, and 1000m wide, respectively. The other variables are taken from *Hirth et al (2001):* $f_{H_2O}^{m}$ is water fugacity to power m, where m=1 and $f_{H_2O} = 37MPa$. The stress exponent n=4, and prefactor k =$10^{-11.2}$ MPa^{-n}/s. The activation energy is taken as Q=135KJ/mol. One can see that these lines intersect the exponential creep law before they intersect the friction curve. The exact location of this transition between exponential creep and power-law creep depends on slip rate, shear zone width, and other model parameters (not shown). Below the exponential to power law transition, power-law creep dominates the deformation since it predicts lower strength for the same slip rate.

Thus we have three zones, a shallow frictional zone which at a well defined depth gives way to the frictional -plastic transition zone, characterized by the low temperature exponential flow law which in turn gives way, at greater depth, to a power law creep regime characteristic of high temperature plastic flow. The BDT thus does not occur at a point, but over a width characterized by a span of temperatures. This is just as expected by experimental studies on quartz plasticity [*Hirth and Tullis*, 1992], who found that this transition zone, from the onset of plasticity to a regime consistent with power law creep, spanned 200°C, independent of strain rate. The best field observations of this transition are from [*Stipp et al.*, 2002], who observed this transition on the Tonale fault in the Italian Alps. They found that the lower transition, the onset of plasticity, occurred at ~300°C. The upper transition to a flow regime consistent with power law creep occurred at ~500°C. The Tonale fault is a 250 km long strike-slip transform segment between two thrusts of the Periadriadriatic fault system. Its strength-depth profile should therefore correspond to that of a thrust fault. It accommodated at least 30 km of slip during its active period in the Oligocene [*Muller et al.*, 2001]. The Tonale fault is thus probably best placed in the fast intraplate fault category (3mm/yr). The width of its shear zone is about 300 m *[Stipp et al, 2002]*. At that slip velocity and width Figure 6 indicates that the lower transition point is at 12 km depth and the upper transition at 18 km. Those depths correspond to temperatures of 300 and 450°C, respectively, in very good agreement with the field and experimental data.

ii. Interactions between seismic and interseismic deformation, as predicted by the model.

The assumption that plasticity onset is controlled by real contact area saturation, predicts a certain depth for the transition from frictional sliding to exponential creep, as discussed in the previous subsection. When using a normal geotherm of 25C/km this depth is ~11kms (fig 5), but the onset of the BDT will be deeper (shallower) in colder (hotter) locations. The BDT zone predicted by our model is a zone where plastic slip co-exists with frictional slip: Plasticity dominates low slip rates while frictional slip dominates fault slip at fast rates. The co-existence of two sliding mechanisms, predicted to occur at the same depth but for faults sliding at different rates, may explain shear zones that exhibit seemingly surprising assemblages of micro-structures and behaviors.

Fig 7 depicts our suggestion for the possible lifecycle of fault-zones within the low temperature plasticity zone of the BDT: such fault zones may creep plastically for a long time as mylonites at the bottom of seismogenic fault zones (point 1 in Fig 7). A large earthquake initiating above the BDT can then propagate below it by virtue of increasing the slip velocity there, driving it into the velocity-weakening frictional regime (2). Unstable slip then leads acceleration to coseismic slip rates that produce melting – and the resulting pseudotachylytes (3). After slip ceases and the fault cools, the fault returns to state (1) and resumes plastic flow, resulting of mylotinization of the pseudotachylytes.

Many observations of fault zones just below the BDT show pseudotachylytes penetrating into mylonites (*Camacho et al., 1995; Lin et al., 2005; Passchier, 1984). Lin et al. (2005)* describe pseudotachylytes in the Woodroffe thrust, Western Australia, within a 1.5 km thick mylonitized shear zone separating granulite facies from amphibolite facies gneisses. The shear zone, exposed at a depth of 25–30 km, contains large volumes of millimeters to centimeter scale pseudotachylyte veins. They are of two types, cataclasite related, and mylonite related. The pseudotachylyte veins penetrate into mylonites and ultramylonites and are themselves overprinted by subsequent mylonitization, with foliation parallel to that of the mylonites. The cataclastic-related veins overprint the mylonite-related ones, and were produced subsequent to the unroofing of the fault through the brittle-plastic transition.

We suggest that observations of seemingly cogenetic mylonite–pseudotachylite assemblages may be explained by the cycle depicted in Fig 7. In fact, observations of seemingly cogenetic mylonite–pseudotachylite assemblages are quite common in major fault zones, e.g. the Outer Hebrides Fault Zone *(Sibson 1980),* Redbank Shear Zone, Australia *(Hobbs et al. 1986),* the Silvretta Nappe, Eastern Alps (*Koch & Masch 1992),* and the Møre–Trøndelag Fault Complex in central Norway *(Sherlock et al 2004).* The mylonites and pseudotachylites commonly appear to be syn-kinematic (*White 1996)* and complex formation mechanisms have been proposed to explain their paradoxical co-existence. Our model predicts these relationships in a quite straightforward manner.

6)Discussion

i. Model assumptions for plastic behavior.

Paper 1 developed a model in which friction is determined by thermally activated creep of asperity contacts under steady-state thermal and stress conditions. This paper extends the model to sliding under high ambient temperature and high normal stress, with an additional physical assumption added to capture the transition to plastic shear from purely frictional sliding. We propose that ductility relates to how real contact area evolves during sliding in the following way: thermally activated asperity creep leads to an increasing real area of contact A_r as function of increasing normal stress, temperature, and time (eqn 3c). A_r will eventually reach a maximum value, A_r^{max}, beyond which it cannot increase further. At this point, the shear strength will no longer increase with normal stress, the b term will go to zero, and the rheology will cease to be frictional but will become that of low temperature exponential plastic creep. We call this the friction plastic transition (FPT). The FPT can be expected to depend on minerology. It was observed in room temperature experiments with smectite that at σ_n=30Mpa the b parameter went to zero and the normal stress dependence of strength vanished *[Carpenter et al., 2015; Saffer and Marone, 2003]*.

The value of A_r^{max} and the assumptions of its constancy merit discussion. One might naively expect that A_r^{max}/A grows monotonically until it approaches 1. This supposes that above the FPT the deformation is by volumetrically bulk plastic flow, but an examination of the structure of the materials produced under this condition does not support that contention. The deformed gouge from the high temperature experiments of *Blanpied et al. (1995)* exhibits discrete sliding surfaces, of both the Riedel and C-surface (parallel to the shear direction) types. Thus, even though the rheology is that of plastic flow, deformation is not by bulk flow but largely by shear on discrete surfaces. Such surfaces must have A_r significantly less than A, otherwise they would not be recognizable as surfaces. Natural mylonites also often exhibit discrete slip on c-surfaces (so-called S/C mylonites) and the same inference may be applied to them.

ii. Parameter values.

The parameters of run 4 from paper 1 (see Table 1 above), one of the several sets of parameters used to model the low normal stress and low ambient temperature experiments (Fig 8 of paper 1), were carried over to this paper and used to model the high normal stress and high ambient temperature experiments on granite. With the parameters of run4, our model predicts the results of friction as function of ambient temperature from *Blanpied et al (1995)*, shown in Fig 2. In particular, the model predicts the observed weak thermal strengthening of friction below the frictional plastic transition temperature (T_{FPT}), as well as the pronounced thermal weakening and strong positive slip-rate dependence above T_{FPT}, as seen in the experiments. In addition, the model predicts that the FPT, exhibited as an abrupt change of slope, will depend on slip rate, as seen in Fig 2, and explained in section 6iv below.

All parameters in our model, except the saturated contact area, A_r^{max}, were carried from paper 1, where they were obtained independently using thermodynamic and material parameters. The saturation value for real contact area, A_r^{max}, which is the constant value of real contact area achieved during plastic flow, was the single free parameter used in fitting the model to the experiments of *Blanpied et al (1995).* The best fit, shown in our fig 2, uses run 4 and A_r^{max} =9.5% of A. This value is within a factor of 2 of the value 5% found by *Beeler et al (2016)* (their fig 6).

The three (non-monotonic) curves of *Blanpied et al (1995)* provide multiple and tight constraints on the value of A_r^{max}. The model predicts theoretically (see section 4.i & eqn 9) that the value of A_r^{max} controls both the values of T_{FPT} and the slopes of friction vs temperature curves for T> T_{FPT}: data is reported for 3 different slip rates, and the single A_r^{max}parameter must correctly pinpoint the 3 different temperatures for the FPT transitions, each for a different slip rate. The same A_r^{max}parameter also controls and predicts the 3 different slopes of friction vs T_0 in the plastic regime (eqn 9). The fact that these multiple fits were achieved provides a strong validation of our model, as well as a strong constraint on A_r^{max}. Paper 1 (Fig 8) showed also the good fit of the same model and parameters to low temperature and stress experiments in Tonalite, Novaculite, quartz and granite, as compiled by *DiToro et al (2011).* This lends confidence to the model and also to the assumption that A_r^{max} is a constant independent of T_0.

We stress that at this point there is no theory to calculate the constant A_r^{max}, and such a theory will be an important advancement in the future. In addition, there is also need for measurements of A_r^{max} as function of normal stress, since currently there is only the single set of *Blanpied et al (1995)* measurements at 400MPa.

iii. The frictional-plastic transition relation to the *a* & *b* parameters.

As explained in paper 1, the terms *a* and *b* have a definite physical interpretation revealed by our model: *a* measures the effect of slip rate on contact shear strength, while *b*, measures the effect of time or slip rate on contact area growth. Paper 1 calls *a* the *viscous term* and *b* the *contact area growth term,* based on their physical origin. Paper 1 investigated steady sliding in the frictional regime (under low T & σ_n), deriving from eqns (3) & (4) a frictional law (eqn 6 here) that predicts a generalized form of the empirical Rate and State laws.

In this paper we use this same derivation to investigate sliding at the plastic regime (under high T_0 and σ_n). Our assumption that contact area saturates in plasticity implies that *b* disappears, as seen in the plastic strength eqn (7). Thus in plasticity all effects of area growth, i.e. of the cutoff time t_c and *b*, drop out, leaving only the shear creep effect, described by the viscous term *a*. From eqn (7) one can easily see that in the plastic flow regime $\frac{\partial \mu_{ss}}{\partial \ln(V)} = a$. Since $a > 0$ then, as long as temperature is constant, the viscous term remains velocity strengthening, so plastic slip is velocity strengthening at low and intermediate slip rate. This is in agreement with experimental observations. Only at very high slip rates does thermal-softening take place. Thermal softening is predicted and discussed in eqn 10 of paper 1.

iv. The frictional-plastic transition as function of slip rate

The transition from frictional to plastic behaviors is set in our model by choosing A_r^{max}. We found A_r^{max} by fitting our model to the experimental results in Fig 2. Using this A_r^{max} predicts that slip at geological strain rates, V=10^{-10} m/s, becomes plastic at about 300MPa and 300C, corresponding to ~11kms depth (Fig 5) (i.e. V_{FPT}(300C,300MPa) = 10^{-10} m/s). Shear is plastic only for V< V_{FPT}, while faster slip still is frictional (Fig 5). The reason why plasticity occurs only during slow slip is because slow slip allows contacts sufficient time to grow during their lifetime and reach the saturated contact area, which is the criteria for plasticity onset. The lower panel of Fig 2 shows that as slip rate increases, higher and higher temperatures are required before A_r saturates to A_r^{max}. The same effect of plasticity prevailing at faster slip rates with increasing ambient temperature was also seen experimentally by *Chester and Higgs (1992)*, as shown in Fig 1b.

As ambient temperatures and normal stress rise with depth in the crust, contact growth rate increases (eqn 3c), increasing V_{FPT}, until at ~ 400MPa and 480C, (representing 15km depth), slip is plastic at all slip rates, and V_{FPT} is in the range of co-seismic velocities. At this depth even the fastest sliding faults have saturated contact area.

v. Friction as function of temperature.

Run 4 fits both the rise of friction with ambient temperature before the FPT and the drop of strength with ambient temperature after the FPT, following closely the data of *Blanpied at el. (1995),* as seen in Fig 2. Not all of the runs that fit the low T, low σ_n data in Paper 1 fit the high T & high σ_n data so well. In the crudest sense, the data in fig 2 poses two constraints: in the frictional regime friction must increase with T_0, while in the plastic regime strength should decrease with T_0. From eqns 6&7 one can calculate $\frac{\partial \mu_{ss}}{\partial T}$ in the two regimes, and see when these constrains are fulfilled:

$$(10a) \qquad \frac{\partial \mu_{ss}^{f}}{\partial T_c} \sim \frac{\partial a}{\partial T_c} \ln\left(\frac{V}{V_{smax}}\right) - \frac{\partial b}{\partial T_c} \ln\left(\frac{t_c V}{d}\right) > 0$$

and

$$(10b) \qquad \frac{\partial \mu_{ss}^{p}}{\partial T_c} \sim \frac{\partial a}{\partial T_c} \ln\left(\frac{V}{V_{smax}}\right) < 0$$

We shall first analyze the plastic regime, eqn 10b: using eqn 7 we see that $\frac{\partial a}{\partial T_c} = \mu_0^p \frac{R}{Q_s}$ with $\mu_0^p = \frac{A_r^{max}}{A\sigma_n} \frac{Q_s}{N\Omega_s}$ (all positive parameters). Since $V_{smax} \gg V$, then all minerals fulfil the condition in eqn (10b) that $\frac{\partial \mu_{ss}^p}{\partial T_c} < 0$, exhibiting thermal softening in plastic flow. In fact, eqn(10b) predicts a material–independent *linear* drop of strength with ambient temperature in the plastic regime. This is what gives rise to the linear drop in strength with depth in Fig. 6. The linear drop of μ_{ss}^p with T_0 predicted in eqn(10b) and fitting fig 2, depends on the assumption that $A_r^{max} = const.$ If A_r^{max} grows with T_0, then $\frac{\partial a}{\partial T_c}$ will not be constant and there will not be a linear trend.

Next we look at the frictional regime: The data-dictated condition in eqn (10a), i.e. that $\frac{\partial \mu_{ss}^f}{\partial T_c} > 0$ in the frictional regime, is less trivial and is only met under certain values of the *a&b* pre-factors. In fact, when plugging in parameters values from Table 1, it is concluded that without considering the temperature dependence of σ_c^0, this condition is not met and $\frac{\partial \mu_{ss}^f}{\partial T_c} < 0$. Friction is thermally strengthening in the frictional regime only if one also considers the temperature dependence of σ_c^0, i.e. the temperature dependence of the indentation stress at t=0. This dependence is in turn dictated in our model by the B parameter dependence on T_0, as discussed in paper 1. We used here, and in paper 1, experimental σ_c^0 dependence on T_0 taken from quartz indentation experiments of *Evans (1984),* his fig 5, which was enough to ensure the thermal strengthening observed here in the frictional regime.

One may ask why here in Fig 2 the high T experiments show thermal strengthening in the frictional regime, while in paper 1, the low T & low normal stress experiments show thermal softening at high velocities. As explained above, plugging parameters values from Table 1 in eqn 10a predicts that thermal softening will prevail, unless σ_c^0 , the indentation stress on contacts, decreases rapidly with increasing temperature. (In other words, strengthening is obtained only if one assumes the contact area at time of contact initiation increases with increasing T_0). In fitting the low T_0 experiments in paper 1, σ_c^0 was taken constant since we assumed contacts heated up only during sliding, and are initially cold at the first nano-second of any two contacts meeting. In contrast, here under elevated T_0, the temperature dependence of σ_c^0 was taken into account, and we used σ_c^0 that decreases with T_0, following fig 5 of *Evans (1984).*

vi. Comparison to others work

Previous work has attempted to fit high T and high normal stress experiments mostly via empirical laws and functional fitting: *Blanpied et al (1995)* fit their data using the R/S friction law to which was added an empirical temperature dependence due to *Chester (1994,1995).* This was originally developed to fit the data of *Chester and Higgs (1992). Shimamoto and Noda (2014)* represent the friction-plastic transition by a ratio of macroscopic empirical laws for friction and flow with a smooth transition by a *tanh* function. These models are not qualitatively different from the two-state model such as *Brace & Kolstedt (1980).* They can fit the data but do not contain a theory that predicts the data.

References

1. Baumberger, T., & Caroli, C. (2006). Solid friction from stick–slip down to pinning and aging. Advances in Physics, 55(3-4), 279-348.
2. Beeler, N. M., Tullis, T. E., & Goldsby, D. L. (2008). Constitutive relationships and physical basis of fault strength due to flash heating. JGR: Solid Earth (1978–2012), 113(B1).
3. Beeler, N. M., G. Hirth, A. Thomas, and R. Bürgmann (2016), Effective stress, friction, and deep crustal faulting, J. Geophys. Res. Solid Earth, 121, 1040–1059, doi:10.1002/2015JB012115,
4. Bowden, F. P., & Tabor, D. (1956). The friction and lubrication of solids
5. Bowden, F. P., & Tabor, D. (1964). The friction and lubrication of solids (Vol. 2, No. 2). Oxford: Clarendon press.
6. Blanpied, M. L., Lockner, D. A., & Byerlee, J. D. (1995). Frictional slip of granite at hydrothermal conditions. JGR: Solid Earth (1978–2012), 100(B7), 13045-13064.
7. Brace, W. F., & Kohlstedt, D. L. (1980). Limits on lithospheric stress imposed by laboratory experiments. Journal of Geophysical Research: Solid Earth, 85(B11), 6248-6252.
8. Brechet, Y., Estrin, Y., (1994). The effect of strain rate sensitivity on dynamic friction of metals. Scripta Met. Mater. 30, 1449–1454.

9. Camacho, A., R. H. Vernon, and J. D. Fitz Gerald (1995), Large Volumes of Anhydrous Pseudotachylyte in the Woodroffe Thrust, Eastern Musgrave Ranges, Australia, Journal of Structural Geology, 17(3), 371-383.

10. Carpenter, B. M., D. M. Saffer, and C. Marone (2015), Frictional properties of the active San Andreas Fault at SAFOD: Implications for fault strength and slip behavior, JGR-Solid Earth, 120(7), 5273-5289, doi:10.1002/2015jb011963.

11. Chester, F. M. (1994). Effects of temperature on friction: Constitutive equations and experiments with quartz gouge. JGR: Solid Earth (1978–2012), 99(B4), 7247-7261

12. Chester, F. M. (1995). A rheologic model for wet crust applied to strike-slip faults. JGR, 100, 13033-13033.

13. Chester, F. M., & Higgs, N. G. (1992). Multimechanism friction constitutive model for ultrafine quartz gouge at hypocentral conditions. JGR: Solid Earth, 97(B2), 1859-1870.

14. Dieterich, J. H. (1972), Time-dependent friction in rocks, J. Geophys. Res., 77, 3690– 3697.

15. Dieterich, J. H. (1978). Time-dependent friction and the mechanics of stick-slip. Pure and applied geophysics, 116(4-5), 790-806.

16. Di Toro, G., Goldsby, D. L., & Tullis, T. E. (2004). Friction falls towards zero in quartz rock as slip velocity approaches seismic rates. Nature, 427(6973), 436-439..

17. Di Toro, G., Han, R., Hirose, T., De Paola, N., Nielsen, S., Mizoguchi, K., ... & Shimamoto, T. (2011). Fault lubrication during earthquakes. Nature, 471(7339), 494-498.

18. Evans, B., & Goetze, C. (1979). The temperature variation of hardness of olivine and its implication for polycrystalline yield stress. Journal of Geophysical Research: Solid Earth (1978–2012), 84(B10), 5505-5524.

19. Evans, B. (1984). The effect of temperature and impurity content on indentation hardness of quartz. Journal of Geophysical Research: Solid Earth (1978–2012), 89(B6), 4213-4222.

20. Goetze, C., & Evans, B. (1979). Stress and temperature in the bending lithosphere as constrained by experimental rock mechanics. Geophysical Journal International, 59(3), 463-478.

21. Hanley, E. J., Dewitt, D. P., & Roy, R. F. (1978). The thermal diffusivity of eight well-characterized rocks for the temperature range 300–1000 K. Engineering Geology, 12, 31-47.

22. Heslot, F., Baumberger, T., Perrin, B., Caroli, B., Caroli, C., 1994. Creep, stick-slip, and dry friction dynamics: experiments and a heuristic model. Phys.Rev.E 49, 4973–4988.

23. Hirth, G., & Tullis, J. (1992). Dislocation creep regimes in quartz aggregates. Journal of Structural Geology, 14(2), 145-159.

24. Hirth, G., Teyssier, C., & Dunlap, J. W. (2001). An evaluation of quartzite flow laws based on comparisons between experimentally and naturally deformed rocks. International Journal of Earth Sciences, 90(1), 77-87.

25. Hobbs, B. E., Ord, A., & Teyssier, C. (1986). Earthquakes in the ductile regime?. Pure and Applied Geophysics, 124(1-2), 309-336.

26. Hull, J. (1988). Thickness-displacement relationships for deformation zones. Journal of Structural Geology, 10(4), 431-435.

27. Koch, N., & Masch, L. (1992). Formation of Alpine mylonites and pseudotachylytes at the base of the Silvretta nappe, Eastern Alps. Tectonophysics, 204(3), 289-306.

28. Lin, A. M., T. Maruyama, S. Aaron, K. Michibayashi, A. Camacho, and K. I. Kano (2005), Propagation of seismic slip from brittle to ductile crust: Evidence from pseudotachylyte of the Woodroffe thrust, central Australia, Tectonophysics, 402(1-4), 21-35.

29. Mei, S., Suzuki, A. M., Kohlstedt, D. L., Dixon, N. A., & Durham, W. B. (2010). Experimental constraints on the strength of the lithospheric mantle. JGR: Solid Earth, 115(B8).

30. Müller, W., Prosser, G., Mancktelow, N. S., Villa, I. M., Kelley, S. P., Viola, G., & Oberli, F. (2001). Geochronological constraints on the evolution of the Periadriatic Fault System (Alps). International J of Earth Sci., 90(3), 623-653.

31. Nakatani, M. (2001). Conceptual and physical clarification of rate and state friction: Frictional sliding as a thermally activated rheology. JGR: Solid Earth (1978–2012), 106(B7), 13347-13380.

32. Nakatani, M., & Scholz, C. H. (2004a). Frictional healing of quartz gouge under hydrothermal conditions: 1. Experimental evidence for solution transfer healing mechanism. JGR: Solid Earth (1978–2012), 109(B7).

33. Nakatani, M., & Scholz, C. H. (2004b). Frictional healing of quartz gouge under hydrothermal conditions: 2. Quantitative interpretation with a physical model. JGR: Solid Earth (1978–2012), 109(B7).

34. Noda, H. (2008). Frictional constitutive law at intermediate slip rates accounting for flash heating and thermally activated slip process. Journal of Geophysical Research: Solid Earth (1978–2012), 113(B9).

35. Passchier, C. (1984), The generation of ductile and brittle deformation bands in a low-angle mylonite zone, J. Struct. Geol., 6, 273-281.

36. Putelat, T., Dawes, J. H., & Willis, J. R. (2011). On the microphysical foundations of rate-and-state friction. J Mech. & Phys. Solids, 59(5), 1062-1075.

37. Rice, J. R., Lapusta, N., & Ranjith, K. (2001). Rate and state dependent friction and the stability of sliding between elastically deformable solids. J Mech. & Phys. Solids, 49(9), 1865-1898.

38. Rice, J. R. (2006). Heating and weakening of faults during earthquake slip. Journal of Geophysical Research: Solid Earth (1978–2012), 111(B5).

39. Saffer, D. M., and C. Marone (2003), Comparison of smectite- and illite-rich gouge frictional properties: application to the updip limit of the seismogenic zone along subduction megathrusts, Earth and Planetary Science Letters, 215(1-2), 219-235, doi:10.1016/s0012-821x(03)00424-2

40. Sibson, R. H. (1980). Transient discontinuities in ductile shear zones. Journal of Structural Geology, 2(1-2), 165-171.

41. Sibson, R. H. (1982). Fault zone models, heat flow, and the depth distribution of earthquakes in the continental crust of the United States. Bulletin of the Seismological Society of America, 72(1), 151-163.

42. Sherlock, S. C., Watts, L. M., Holdsworth, R. E., & Roberts, D. (2004). Dating fault reactivation by Ar/Ar laserprobe: an alternative view of apparently cogenetic mylonite–pseudotachylite assemblages. Journal of the Geological Society, 161(3), 335-338.

43. Shimamoto, T., & Noda, H. (2014). A friction to flow constitutive law and its application to a 2□D modeling of earthquakes. JGR: Solid Earth, 119(11), 8089-8106.

44. Stipp, M., StuÈnitz, H., Heilbronner, R., & Schmid, S. M. (2002). The eastern Tonale fault zone: a 'natural laboratory'for crystal plastic deformation of quartz over a temperature range from 250 to 700 C. Journal of Structural Geology, 24(12), 1861-1884.

45. Tsenn, M. C., & Carter, N. L. (1987). Upper limits of power law creep of rocks. Tectonophysics, 136(1), 1-26.

46. Voll, G. (1976), Recrystallization of quartz, biotite, and feldspars from Erstfeld to the Levantina nappe, Swiss Alps, and its geological implications, Schweiz. Miner. Petrogr. Mitt., 56, 641-647.

47. Vosteen, H. D., & Schellschmidt, R. (2003). Influence of temperature on thermal conductivity, thermal capacity and thermal diffusivity for different types of rock. Physics and Chemistry of the Earth, Parts A/B/C, 28(9), 499-509.

48. White, S., Burrows, S., Carreras, J., Shaw, N., and Humphreys, F. (1980), On mylonites in ductile shear zones, J. Struct. Geol., 2, 175-187.

49. White, J. C. (1996). Transient discontinuities revisited: pseudotachylyte, plastic instability and the influence of low pore fluid pressure on deformation processes in the mid-crust. Journal of Structural Geology, 18(12), 1471-1486.

Figures

(a)

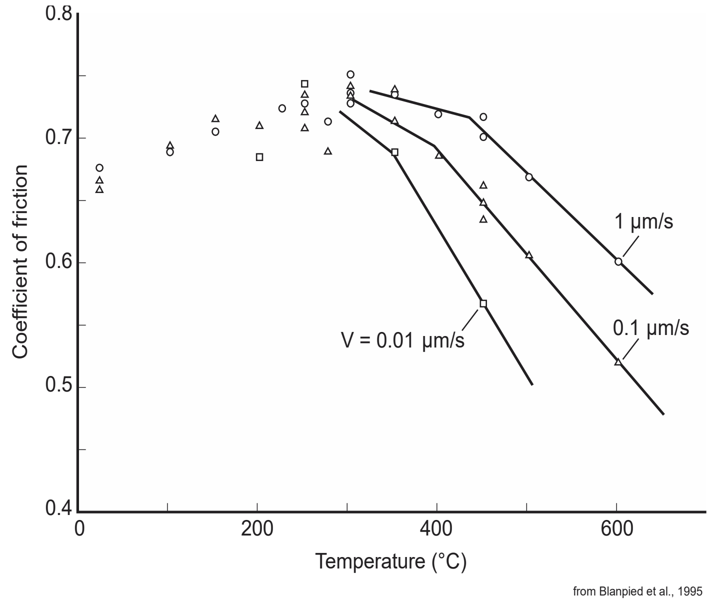

(b)

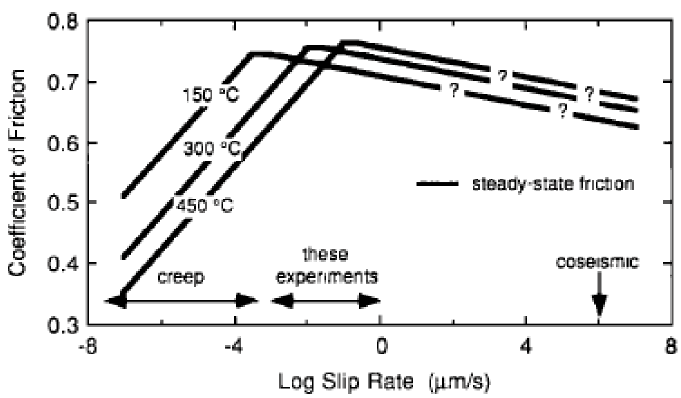

Fig 1: A) Experimental friction of wet granite as function of ambient temperature T_0, for three different slip rates, from *Blanpied et al (1995)*. Below ~300C, friction increases with T_0, and is independent of slip rate. For T_0 greater than ~ 300C, friction decreases with increasing T_0, but increases strongly with increasing slip rate. B) Figure 9 from Chester and Higgs (1992): Steady state friction versus log slip rate for different temperatures in wet ultrafine quartz gouge experiments. Behavior at low slip rates is dominated by plastic flow, whereas at high slip rates it is dominated by frictional slip. The transition between mechanisms is indicated by change in the

slope of the lines. The transition occurs at higher slip rates for increasing temperatures. Behavior at very high slip rates was uncertain at that time.

(a)

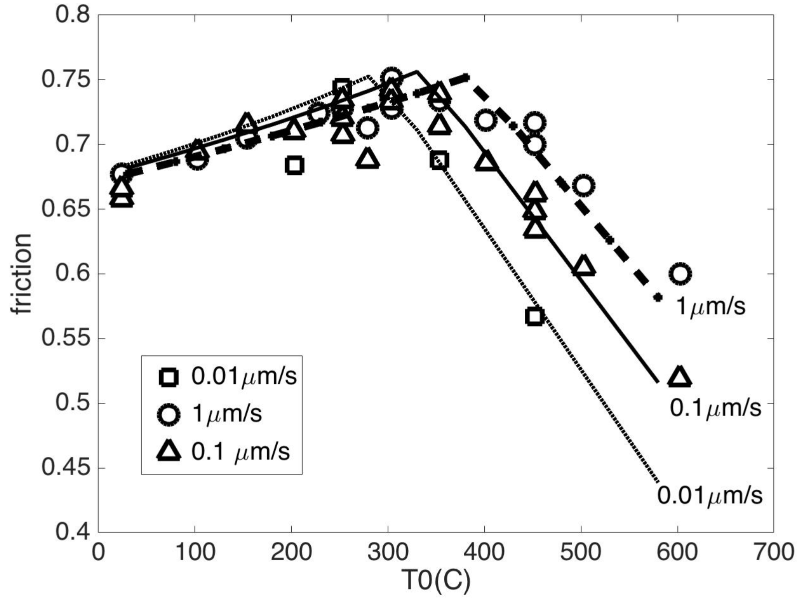

(b)

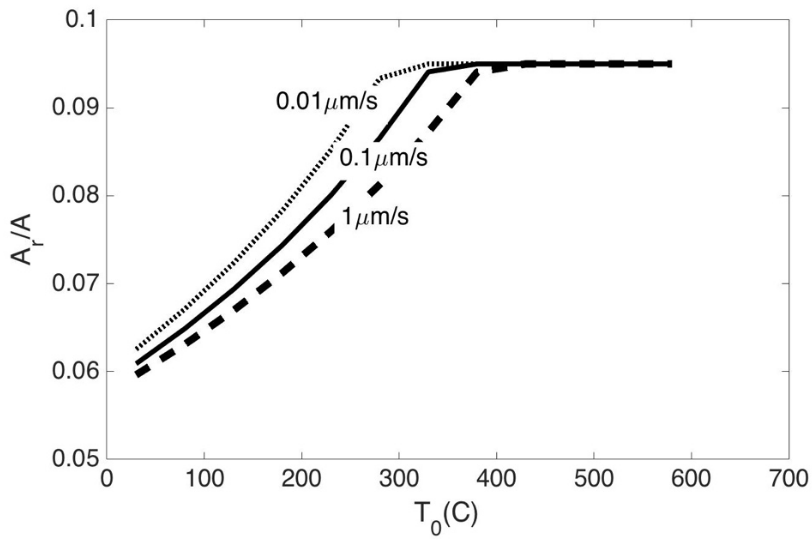

Fig 2: a): Experimental friction of wet granite as function of ambient temperature, T_0, for 3 different slip rates, from *Blanpied et al (1995),* in symbols (same data as in Fig 1a). Note that the y-axis, though labeled friction, is shear stress divided by a constant normal stresss of 400 MPa. In the frictional regime it is appropriate to refer to this as the friction coefficient, but in the plastic regime it should be referred to as the shear strength. Model results in lines. The temperature of the friction-plastic transition (FPT), $T_{FPT,}$ appears here as a peak in friction, whose position is a function of slip rate. For $T_0<T_{FPT}$ friction increases with T_0, but is nearly

independent of slip rate (only second-order Rate and State effects). For T_0>T_{FPT} the strength decreases strongly with ambient temperature, yet increases with slip rate. Parameters of run 4 (see Table 1) were used since they presented the best fit.

b): Normalized contact area vs T_0, for the same 3 slip rates. Contact area increases with increasing $T_{0,}$ until it saturates to A_r^{max}, at which point the system undergoes a FPT. T_{FPT} increases with slip rate, since slower sliding contacts have more time for contact area growth, resulting in a larger contact area for a given T_0.

(a)

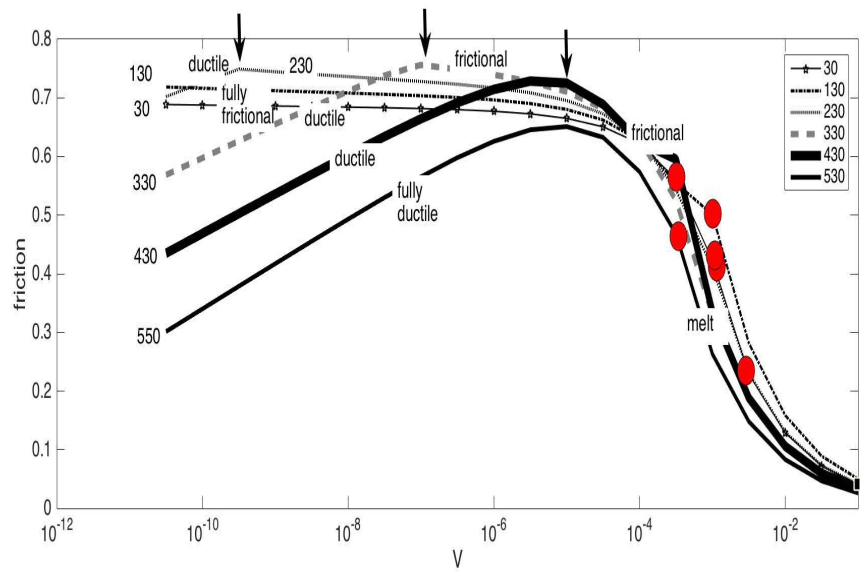

(b)

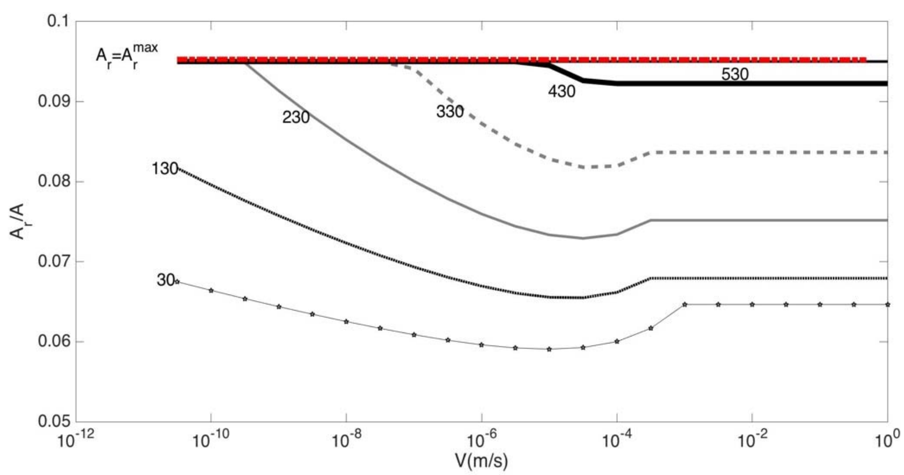

Fig 3: (a) Model results for steady-state friction as function of slip rate V (m/s), for various ambient temperatures (T_0 noted in degrees Celsius on each curve), at σ_n=400MPa. Below 230°C

sliding is fully frictional. At 230°C slip becomes plastic for V< 0.001 μm/s. As T_0 increases, plasticity extends to higher and higher slip rates, until at 550°C sliding is fully plastic at all slip rates. At this high temperature, although sliding is fully plastic, still thermal-weakening sets in at high enough V. Arrows indicate the FPT for each curve

(b) Normalized real contact area, A_r/A for runs in (a). Note that at this high stress real contact area is large, a few percent of A. The red line depicts the maximum contact area determined from fitting the experiments of Fig 2. Below 230°C sliding is fully frictional, presenting a variable contact area with slip rate. Slip becomes plastic, i.e. $A_r=A_r^{max}$, at 230°C but only for very slow slip, for V< 0.001 μm/s. As T_0 increases, plasticity is achieved at higher and higher slip rates, until at 550°C sliding is fully plastic at all slip rates, seen here as sliding at A_r^{max} at all slip rates.

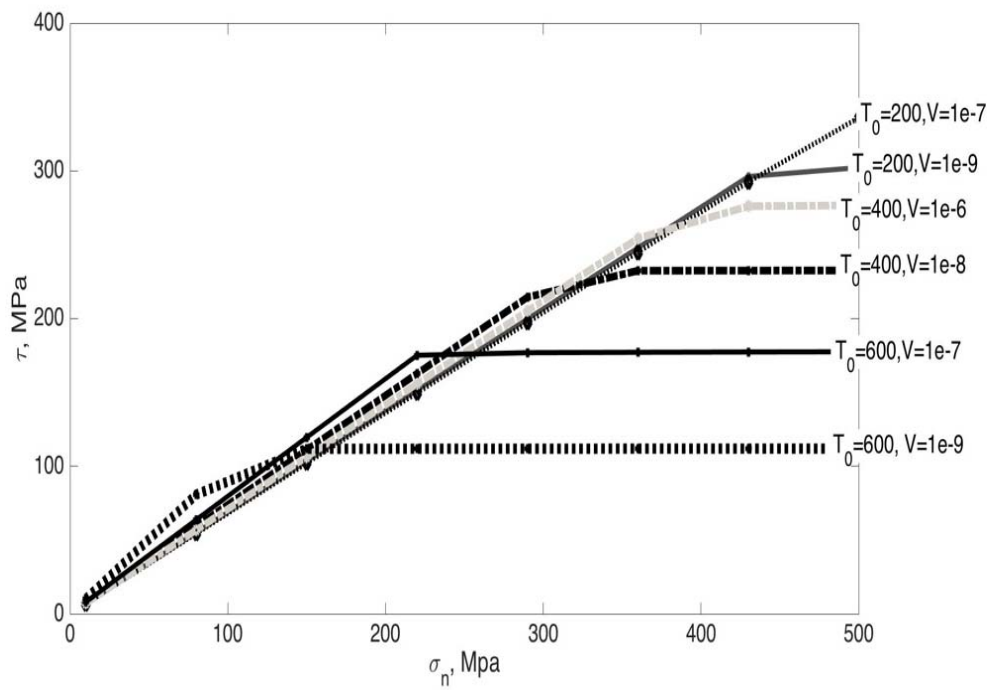

Fig 4: model results for shear stress at a given slip rate and ambient temperature (noted on RHS, units are degrees C and m/s) versus the applied normal stress. The frictional -plastic transition appears as a transition from linear dependence between shear stress and normal stress (eqn 6d) to constant shear stress, independent of normal stress (eqn 7c). The normal stress at which the FPT occurs increases with decreasing T_0 and increasing slip rate as explained in Fig 2b.

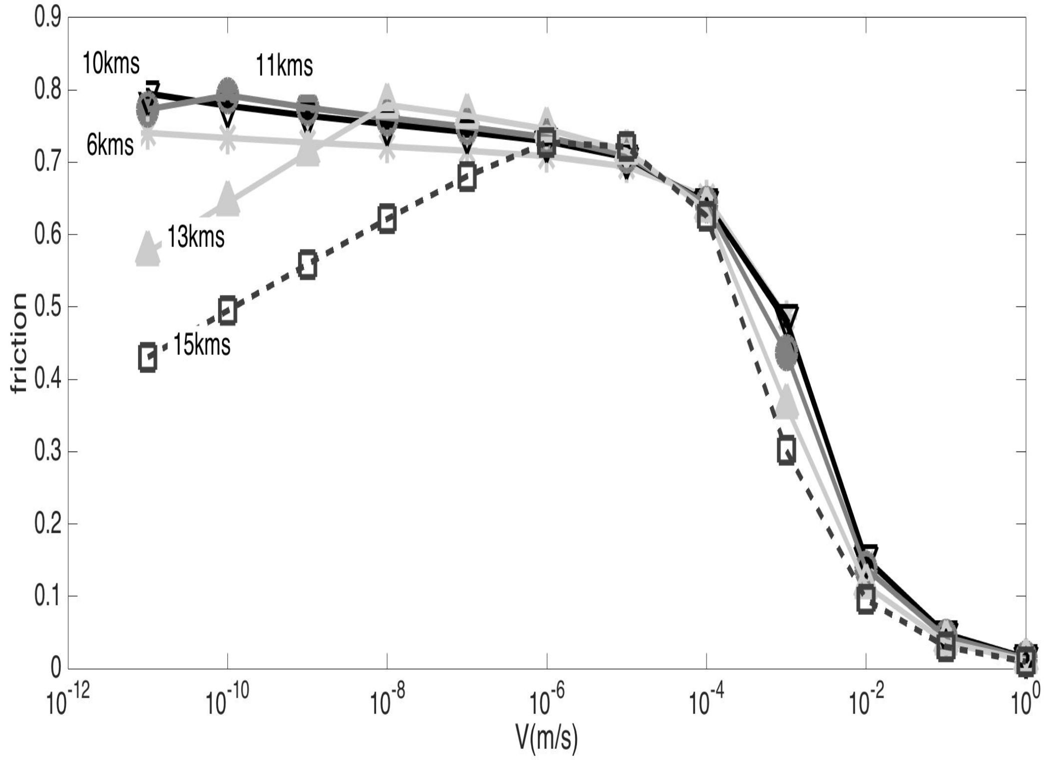

Fig 5: friction in quartz/granite, modeled using parameters of run4, as function of V, for different depths in the crust. Ambient temperature and normal stress for each curve are calculated from geothermal and stress gradients of 25C/km and 18MPa/km respectively. Descending from the surface to 10kms, the friction coefficient increases slightly but also becomes increasingly velocity weakening with depth. Below 10kms, granite creeps plastically at very slow (geological) slip rates, but still slides frictionally, and thermally weakens when sliding faster. This is seen as a change in slope at the FPT slip rate, V_{FPT}. $V_{FPT} = 10^{-10}$m/s=0.0001μm/s at 11kms. Going deeper, ductility dominates higher and higher slip rates, so V_{FPT} =0.01μm/s at 13 kms depth. Sliding at 15kms is fully-plastic, yet shear heating causes thermal softening at V >5 μm/s.

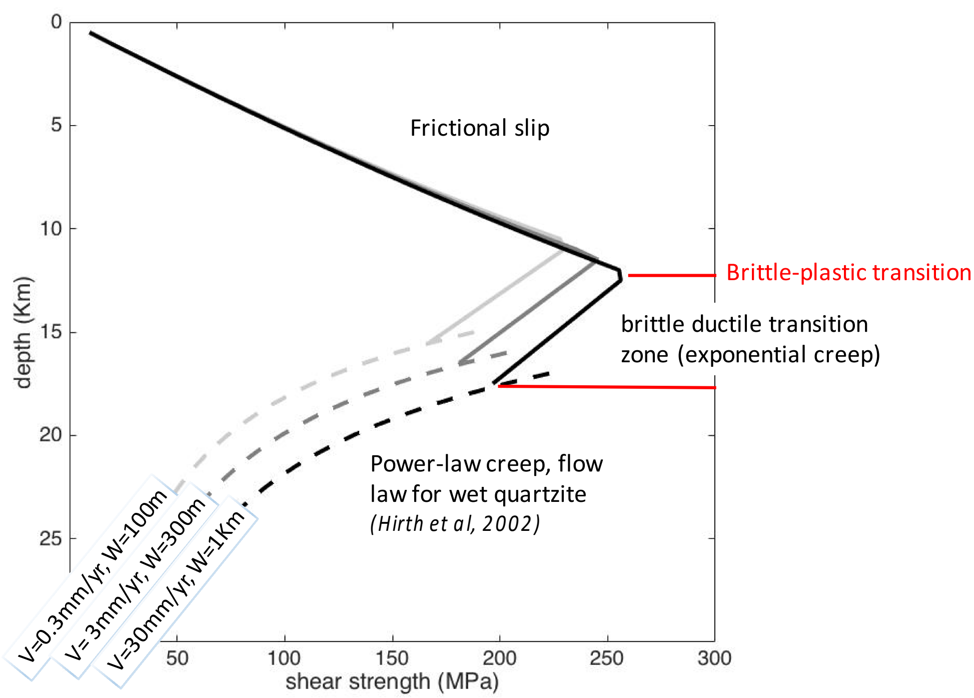

Fig 6: Quartz/granite shear strength as function of depth, for three different geological slip rates (0.3, 3 and 30 mm/yr) representing geologic slip rates for active faults. These rates correspond to slow intraplate, fast intraplate, and interplate faults, respectively. The solid lines are our model calculations. The dashed lines are power-law wet quartzite experimental flow laws (Hirth et al, 2001), as detailed in eqn10. Our model shows a transition from friction to exponential creep at a depth that increases with the slip rate, between 11-14 kms. Exponential creep then extends down until it intersect the power-law creep flow law. The exact location of this transition between exponential creep and power-law creep depends on slip rate, shear zone width, and other model parameters (not shown). Below the exponential to power law transition, power-law creep dominates the deformation since it predicts lower strength for the same slip rate. Thus we predict a FPT transition zone that ranges from 11kms to 20kms, depending on conditions. This transition zone is characterized by plastically–sliding faults which are predicted to merge into shear zones at greater depth.

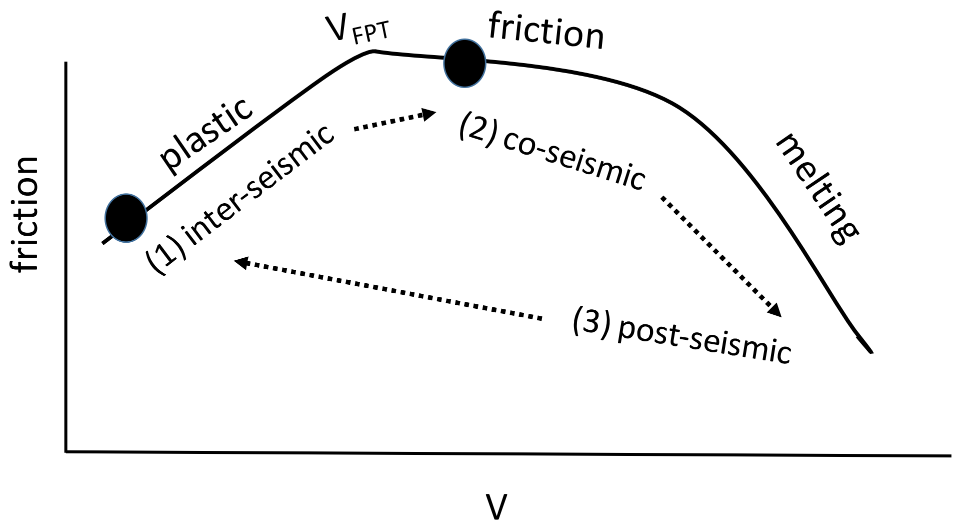

Fig 7: cartoon illustrating lifecycles of a fault at a depth somewhat below the BDT, inferred from model predictions. This cartoon redraws the friction-velocity dependence of fig 5, which shows that for normal geothermal conditions, at, say,13kms sliding at high strain rate will occur by frictional slip and exhibit velocity weakening, while slow slip occurs in plastic manner. Thus, deeply buried fault zones, beneath the BDT of seismogenic faults, spend most of their lifetimes between earthquakes, sliding plastically as mylonites (point 1). A large earthquake that nucleates on the fault above the BDT zone may propagate downwards into the BDT zone and drive motion to a slip rate that is within the frictional regime (point 2). This regime allows unstable sliding due to the velocity and thermal weakening behavior that exists for sliding at V> VFPT. The fault will accelerate to co-seismic slip rates, resulting in melting and the production of pseudotachylytes. After the earthquake is finished the fault decelerates and cools (point 3), and sliding returns quite quickly to its inter-seismic mode (point 1), resuming plastic deformation.